29 October 1999

ELSEVIER

Chemical Physics Letters 312 (1999) 598–605

CHEMICAL PHYSICS LETTERS

www.elsevier.nl/locate/cplett

Origin of the unusual stability of MnO_4^-

Gennady L. Gutsev [a], B.K. Rao [a,*], P. Jena [a], Xue-Bin Wang [b,c], Lai-Sheng Wang [b,c]

[a] *Physics Department, Virginia Commonwealth University, Richmond, VA 23284-2000, USA*
[b] *Department of Physics, Washington State University, Richland, WA 99352, USA*
[c] *W.R. Wiley Environmental Molecular Sciences Laboratory, Pacific Northwest National Laboratory, MS K8-88, P.O. Box 999, Richland, WA 99352, USA*

Received 19 May 1999; in final form 29 August 1999

Abstract

The attachment of an electron to manganese tetroxide cluster is found to lower its total energy by as much as 5 eV, thus putting MnO_4 into the class of superhalogens. This result, predicted by first-principles calculations based on density functional theory and generalized gradient approximation, is verified experimentally by photodetachment spectroscopy. The combined theoretical and experimental studies not only allow a fundamental understanding of the origin of the unusual stability of MnO_4^- but also provide information on ground-state geometries, vibrational frequencies, and electronic structure of MnO_4, MnO_4^-, and their isomers.

We report the first observation of a transition-metal cluster compound whose electron affinity (EA) is significantly larger than that of atomic chlorine, the most electronegative element in the Periodic Table. This compound, consisting of one manganese and four oxygen atoms (MnO_4), has an electron affinity of 5 eV and thus belongs to the class of superhalogens [1]. The origin of the unusual stability of MnO_4^- is due to the existence of Mn in a $+7$ valence state. With oxygen being divalent, the electronic structure of MnO_4 is characterized by a hole in the outermost shell. The chemistry of MnO_4, therefore, mimics the chemistry of halogen atoms, but its larger size compared to the chlorine atom enhances its electronegativity. The existence of Mn in its maximal valence configuration is also manifested in the magnetic character of MnO_4^-. It has zero magnetic moment while Mn atom, as well as MnO, carries a moment of 5 μ_B. This understanding is important because the interaction of manganese with oxygen plays a prominent role in inorganic chemistry, as well as in biologically important metallo-enzymes. For example, the permanganate anion, MnO_4^-, is a very common inorganic anion in solutions and solids and is extensively used as an oxidizing agent [2]. Similarly, Mn–dimer oxocomplexes are sub-units in metallo-enzymes.

Although extensive studies of MnO_4^- have been carried out in the condensed phases and solutions [2], very few studies of MnO_4^- in the gas phase have been reported [3–5]. We have carried out a combined first-principles theoretical and experimental study of MnO_4^- and MnO_4 in the gas phase for the first time. The study reveals many novel features of

* Corresponding author. Fax: +1-804-828-7073; e-mail: brao@saturn.vcu.edu

0009-2614/99/$ - see front matter
PII: S0009-2614(99)00976-8

this pair. (1) The neutral MnO_4 cluster has two isomers of C_{2v} symmetry separated in total energy by only 0.18 eV (4 kcal/mol). One of these isomers is a distorted tetrahedron where all four oxygen atoms are bonded to Mn dissociatively. In the other isomer, two of the oxygen atoms remain in a molecular configuration, while the other two are dissociated. (2) Addition of an extra electron to MnO_4 has a dramatic effect on its geometry and stability: MnO_4^- becomes a perfect tetrahedron with all the oxygen atoms bonded to Mn dissociatively. The added electron is distributed uniformly over the four oxygen atoms and the total energy of the neutral parent is lowered by almost 5 eV. (3) The magnetic moments of Mn are quenched from its value of 5 μ_B in Mn and MnO to 1 μ_B and 0 μ_B in MnO_4 and MnO_4^-, respectively. The quantitative agreement between our theory and experiment of the energetics in the photodetachment process allows us to completely understand the origin of the unusual stability of MnO_4^-, demonstrating the power of the current level of theory in explaining experimental data as well as predicting new molecular properties.

Previous theoretical studies have mainly focused on explaining optical excitations in MnO_4^- (see, e.g., Refs. [6,7] and references therein), photochemical decomposition of the anion [8], and its vertical ionization potentials [9]. These studies have assumed the tetrahedral structure of MnO_4^- derived from solutions and salts. To the best of our knowledge, no experimental or theoretical data are available on the structure of the neutral MnO_4 cluster. In the following, we describe our theoretical and experimental approach and discuss the equilibrium geometries, electronic structure, and properties of neutral and anionic MnO_4 in the gas phase.

The calculations are performed using the molecular orbital theory where a linear combination of atomic orbitals centered at various atomic sites constitutes the cluster wave function. Previous authors [10–12] have discussed the failure of the Hartree–Fock approach in treating MnO_4^-. In this work, we have constructed the many-electron potential by using the density-functional theory [13] with the generalized gradient approximation for the exchange-correlation functional. We have used Becke's exchange [14] and Perdew–Wangs' correlation [15] functionals, referred as to BPW91, in the GAUSSIAN 94 software [16]. For the atomic orbitals, we have used the standard 6-311 + G* basis (Mn: [10s7p4d1f]; O: [5s4p1d]). The geometries of the MnO_4 and MnO_4^- isomers for different spin-multiplicities were obtained by minimizing the forces at each atomic site.

The energy of formation of the neutral MnO_4 from two oxygen molecules is calculated using the equation

$$E_b = E_{tot}(Mn) + 2E_{tot}(O_2) - E_{tot}(MnO_4) \quad (1)$$

where $E_{tot}(Mn)$, $E_{tot}(O_2)$, and $E_{tot}(MnO_4)$ are the total energies of Mn, O_2, and MnO_4, respectively. This energy is 6.95 eV. The corresponding energy for MnO_4^-, namely,

$$E_b^- = E_{tot}(Mn) + E_{tot}(O_2) + E_{tot}(O_2^-) - E_{tot}(MnO_4^-) \quad (2)$$

is much higher and equals 11.52 eV. The total energy calculations also enable us to derive the adiabatic electron affinity (A_{ad}) which is defined as the difference in the ground-state total energies of the neutral system and its anion. Within the Born–Oppenheimer (BO) approximation employed in the present work, one may evaluate the A_{ad} as

$$A_{ad} = E_{tot}(N, R_e) + Z_N - E_{tot}(A, R_e^-) - Z_A = \Delta E_{el}^{ad} + \Delta E_{nuc} \quad (3)$$

where R_e and R_e^- denote equilibrium geometries of the neutral system (N) and its anion (A), respectively. The zero-point vibrational energies (Z) are computed within the harmonic approximation. Note that the A_{ad} of O_2 computed at the BPW91/6-311G* level according to Eq. (3) is 0.474 eV. This is in good agreement with the experimental value of 0.451 $\pm$ 0.007 eV [17].

In our experimental investigation, because of an anticipated high binding energy of the extra electron in MnO_4^-, we used an ArF excimer laser (193 nm, 6.424 eV) to measure the photodetachment spectrum. The MnO_4^- was produced from a $KMnO_4$ solution using electrospray. The photoelectron spectrum was measured with a magnetic-bottle time-of-flight (TOF) photoelectron analyzer. Details of this apparatus have been published elsewhere [18] and only a brief description is given here. A 10^{-4} M $KMnO_4$ solution in a methanol/H_2O (98:2) mixed solvent was used

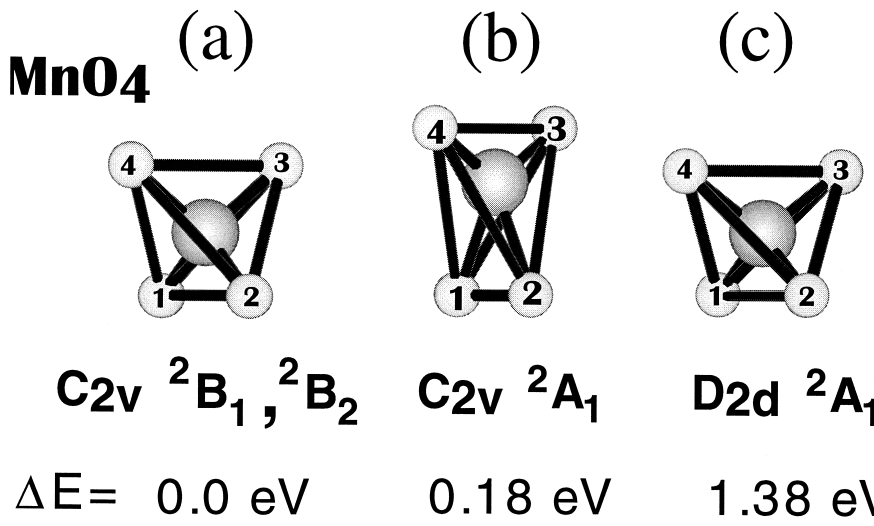

Fig. 1. Geometries of neutral MnO_4, corresponding to the (a) ground state, (b) isomer, nearly degenerate in total energy with the ground state, and (c) higher energy isomer.

in the electrospray. Anions produced in the electrospray source were accumulated in a quadrupole ion trap for 0.1 s before being pulsed out for TOF mass analyses. The detachment laser was operated at 20 Hz with the ion beam off at alternating laser shots for background subtraction. The photoelectron kinetic energy was calibrated with the known spectra of I^- and O^-. The resolution at which the MnO_4^- spectrum was taken was about 30 meV for 1 eV electrons.

In Fig. 1a,b, we give the geometrical configurations of the two isomers of MnO_4 which are nearly degenerate in total energy. The geometry of a higher energy isomer is given in Fig. 1c. The corresponding

Table 1
Results of BPW91/6-311 + G* calculations for ground states of MnO_4 and MnO_4^- and their isomers. Bond lengths (R–X) are in Å, harmonic frequencies are in cm^{-1}, zero-point energies and energy intervals (ΔE_{tot}) are in eV. $O_{1,2}$ and $O_{3,4}$ designate pairs of oxygens equivalent by symmetry

Quantity	MnO_4, $2S+1=2$			MnO_4^-, $2S+1=1$	
	(C_{2v}, $^2B_2$, $^2B_1$)[a] (Fig. 1a)	(C_{2v}, $^2A_1$)[b] (Fig. 1b)	(C_{2v}, D_{2d}, $^2A_1$)[c] (Fig. 1c)	(T_d, $^1A_1$)[d] (Fig. 2a)	(C_{2v}, $^1A_1$)[e] (Fig. 2b)
R(Mn–$O_{1,2}$)	1.641	1.576	1.620	1.620	1.601
R(Mn–$O_{3,4}$)	1.589	1.788	1.620	1.620	1.818
R(O_1–O_2)	2.562	2.675	2.663	2.645	2.767
R(O_3–O_4)	2.611	1.408	2.637	2.645	1.442
R(O_1–O_3)	2.659	2.903	2.663	2.645	2.925
Z	0.30	0.32	0.44	0.35	0.31
ΔE_{tot}	0.0	0.18	1.38	−5.01	−2.91

Vibrational frequencies of the above states of MnO_4 and MnO_4^- are as follows:
[a] $a_1 = 263, 390, 829, 925$; $b_1 = 343, 867$; $a_2 = 285$; $b_2 = 350, 551$.
[b] $a_1 = 337, 577, 960, 1007$; $b_1 = 223, 614$; $a_2 = 230$; $b_2 = 254, 1030$.
[c] $a_1 = 311, 360, 806, 850$; $b_1 = 425, 1751$; $a_2 = 345$; $b_2 = 426, 1764$.
[d] $e = 352$; $t_2 = 400, 932$; $a_1 = 873$.
[e] $a_1 = 320, 605, 914, 943$; $b_1 = 248, 494$; $a_2 = 287$; $b_2 = 257, 972$.

interatomic distances as well as vibrational frequencies corresponding to all normal modes together with relative energies are given in Table 1. Note that the energies are measured with respect to the ground state of MnO_4 (Fig. 1a). The ground state of neutral MnO_4 has a C_{2v} geometry and the $^2B_2$ electronic configuration, which is degenerate with the $^2B_1$ electronic configuration. This geometry represents a distorted tetrahedron with all oxygen–oxygen bonds being around 2.6 Å. The bond length of molecular oxygen, in contrast, is 1.2075 Å [19]. The nearly degenerate isomer that lies 0.18 eV higher in total energy, also has a C_{2v} structure (Fig. 1b) but its two oxygen ligands remain nearly molecular while the other two are dissociative. The electronic state of this isomer is $^2A_1$. We also found a higher energy isomer (Fig. 1c) at 1.38 eV above the ground state that has a D_{2d} structure with all oxygen–oxygen bonds being nearly equal and $^2A_1$ electronic state. All the vibrational frequencies of this high-energy isomer are positive (see Table 1) implying that this structure corresponds to a local minima on the MnO_4 potential energy surface. Thus, it represents an electronic excited state. We will see later that the existence of this excited state is consistent with the photodetachment spectra.

The preferred spin multiplicities of the ground state and isomers of neutral MnO_4 are 2, i.e. each of these clusters carries a magnetic moment of 1 μ_B. However, the distribution of this moment is different for different structures. In the ground state (Fig. 1a), the magnetic moment at the Mn site is -0.31 μ_B. This is antiferromagnetically coupled to moments at the oxygen sites, which are 0.58, 0.58, 0.07, and 0.07 μ_B at sites labeled 1, 2, 3, and 4, respectively (Fig. 1a). On the contrary, in the nearly degenerate peroxide structure (Fig. 1b), Mn carries a moment of 1.16 μ_B with very small antiferromagnetically coupled moments at the oxygen sites. In the higher energy D_{2d} isomer (Fig. 1c), each oxygen atom carries a moment of 0.28 μ_B which is antiferromagnetically coupled to the moment (-0.12 μ_B) at the Mn site.

In Fig. 2, we present the geometry of the ground state of MnO_4^- and its higher energy isomer. The corresponding bond distances, normal mode vibrational frequencies, and relative energies measured with respect to the neutral ground state are given in Table 1. The ground state of MnO_4^- (Fig. 2a) is a perfect tetrahedron with all the oxygen atoms bound to Mn dissociatively and its electronic state is $^1A_1$. Our calculated bond length of 1.620 Å between Mn

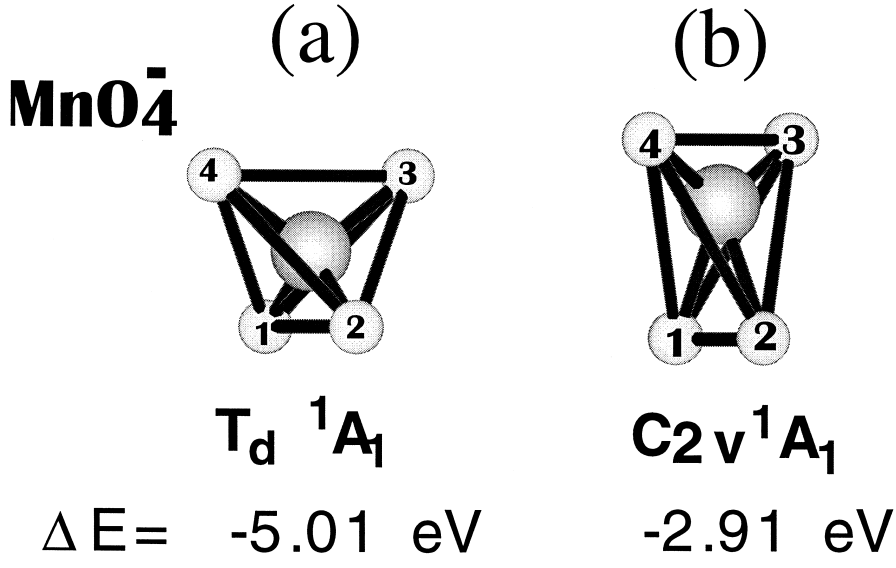

Fig. 2. Geometries of MnO_4^-, corresponding to the (a) ground state and (b) next higher-energy configuration.

and O and vibrational frequencies $\nu(\mathrm{e}) = 352\ \mathrm{cm}^{-1}$, $\nu(\mathrm{t}_2) = 400\ \mathrm{cm}^{-1}$, $\nu(\mathrm{a}_1) = 873\ \mathrm{cm}^{-1}$, and $\nu(t_2) = 932\ \mathrm{cm}^{-1}$ are in good agreement with the experimental bond length of 1.629 ± 0.008 Å [20] and frequencies of 348, 390, 838, and 910 cm^{-1}, respectively, obtained in salts [21].

The total energy of MnO_4^- is lowered by 5.01 eV with respect to the neutral ground state. This yields a very high adiabatic electron affinity of 4.96 eV for MnO_4, according to Eq. (3). This value is much larger than the electron affinity of chlorine, namely, 3.62 eV, which is the highest among all the elements in the Periodic Table. Although certain other transition metal oxides have been found to have electron affinities higher than that of chlorine (e.g., FeO_4 was computed to have the A_{ad} of 3.8 eV [22,23], and the A_{ad} of VO_4 has been measured to be 4.0(1) eV [24]), MnO_4 possesses the largest electron affinity of any transition-metal oxide compound known up to now. This puts MnO_4 into the class of superhalogens [1].

The existence of superhalogens among clusters containing sp-elements has been known for some time. Typical examples include LiF_2, $LiCl_2$, NaF_2, $NaCl_2$, BF_4, AlF_4, PF_6, AlO_2, PO_3, and ClO_4 [25–27]. For a metal oxide with a formula MO_n to behave as a superhalogen, the coordination number n should fulfill the requirement $2n = k + 1$, k being the maximal formal valence of the central atom, M. In the case of MnO_4, the needed valence of Mn to fulfill the superhalogen requirement is $k = 7$. Note that the outermost configuration of Mn is $3d^5 4s^2$, which renders it the maximum formal valence of 7. The fact that the electron affinity of MnO_4 is higher than that of chlorine confirms that the valence of Mn in

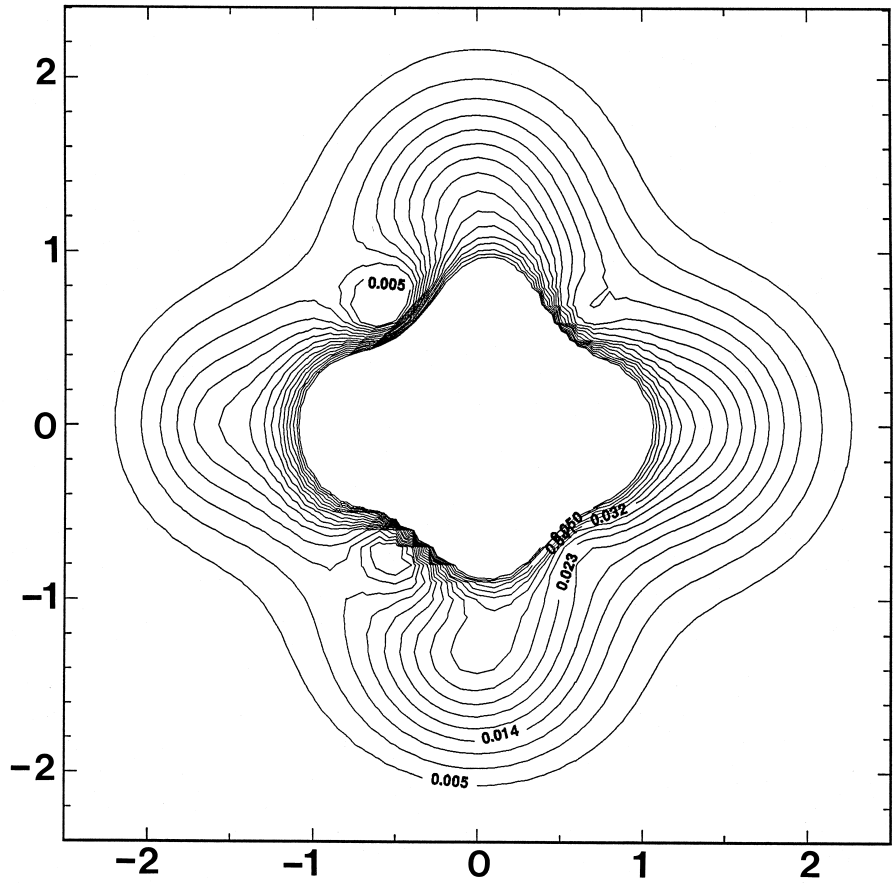

Fig. 3. Charge density difference between MnO_4 and MnO_4^- obtained at the anion ground-state geometry.

this cluster is indeed 7. In MnO_4^-, the extra electron would fill the lowest unoccupied molecular orbital (LUMO) which does not contain contributions from the central atom by symmetry at the anion ground-state geometry. The resulting MnO_4^- anion, thus, has a closed-shell structure and should be thermodynamically and electronically very stable. In Fig. 3, we plot the difference in the charge density between the ground states of MnO_4^- and MnO_4 at the anion geometry. One sees from Fig. 3 that the extra electron in MnO_4^- is distributed uniformly over the four oxygen atoms.

The existence of Mn in its highest $+7$ oxidation state in MnO_4^- manifests itself in its vanishing magnetic moment. To illustrate this, we recall that the $3d^54s^2$ configuration of the Mn atom gives a magnetic moment of 5 μ_B. As one forms a MnO molecule, the $4s^2$ electrons of Mn interact with the 2p electrons of oxygen, leaving the $3d^5$ half-filled shell untouched. As a result, the magnetic moment of MnO is still 5 μ_B [28]. As more oxygen atoms are bound to the Mn atom, its 3d electrons begin to participate in the bonding and all the 3d and 4s valence electrons of Mn hybridize with the 2s and 2p electrons of oxygens in MnO_4^-, thus quenching the magnetic moment to zero.

From the energetics of the neutral and anionic MnO_4, we can compute adiabatic electron affinities that can be compared with the experimental data. The vertical transition from the ground state of MnO_4^- ($^1A_1$, T_d, Fig. 2a) to the $^2B_2$ ground state of MnO_4 (Fig. 1a) yields 5.01 eV, while the vertical transition to the $^2A_1$ state (Fig. 1c) yields 6.39 eV. As will be seen below, these calculated energetics are in excellent agreement with the experimental observation. The vertical transition from the anion ground state to the nearly degenerate neutral configuration (Fig. 1b) would yield 5.19 eV. However, there is too large a geometry change for such a transition; the neutral configuration shown in Fig. 1b is most likely derived from the anion isomer shown in Fig. 2b, with a much lower adiabatic EA of 2.99 eV. As shown below, the low EA peroxide isomer of MnO_4^- was not observed in our photodetachment spectrum because it could not be formed in the electrospray source.

The photodetachment spectrum of MnO_4^- is shown in Fig. 4. The spectral features represent transitions from the ground state of the MnO_4^- anion to the ground and excited states of the neutral MnO_4. Two major detachment features were observed around 5 and 6.1 eV. No other lower binding energy features were observed. Both observed features, labeled X and A, appeared to contain fine structures, either due to overlapping electronic states or vibrational structures. The feature X yields adiabatic and vertical detachment energies of 4.80 (0.10) and 4.91 (0.03) eV, respectively. Because of the lack of vibrational resolution, the adiabatic detachment energy was estimated by drawing a straight line at the

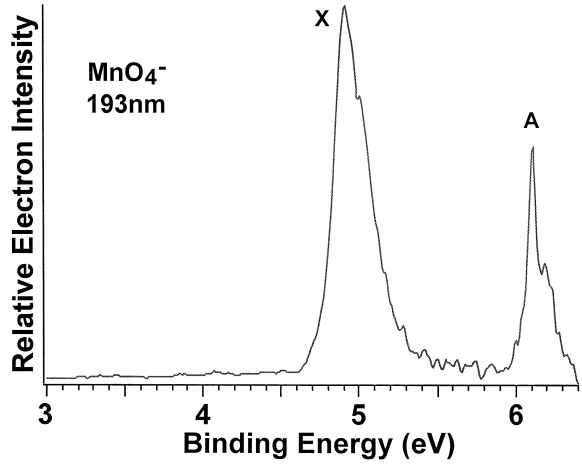

Fig. 4. Experimental photoelectron spectrum of MnO_4^- at 194 nm (6.424 eV).

leading edge of the X feature and then adding a constant to the intersect with the binding energy axis to take into account for the instrumental resolution and possible hot bands. A large uncertainty results from this approximate procedure, as given. The feature A gives rise to adiabatic and vertical detachment energies of 6.05 (0.06) and 6.11 (0.03) eV, respectively. The predicted high EA of MnO_4 is immediately confirmed. The calculated adiabatic EA of 4.96 eV compares well with the measured value of 4.80 eV. Thus the feature X can be assigned to the transition from the ground-state MnO_4^- to the ground state of neutral MnO_4 (Fig. 1a, $^2B_1$, $^2B_2$). The fine structures contained in the feature X are complicated and cannot be assigned to a simple vibrational progression. As can be seen in Table 1, there are four totally symmetric modes for the C_{2v} ground-state MnO_4. It is possible that more than one of these modes is active in the photodetachment transition, giving rise to the more congested vibrational structure. The identified vibrational feature (~ 800 cm^{-1}) is in good agreement with our calculated value of 829 cm^{-1}. It is important to note that even though the neutral ground state has a lower symmetry than the anion ground state the geometrical changes are not great, as seen in Table 1. This observation is also consistent with the relatively narrow observed spectral width.

The photoelectron spectral feature A yields a 6.05 eV adiabatic detachment energy, which is in excellent agreement with the calculated transition energy between the anion and the D_{2d} $^2A_1$ state (6.39 eV). Despite the symmetry changes, Table 1 shows that the structural parameters of the D_{2d} $^2A_1$ state are nearly identical with those of the MnO_4^- ground state, again consistent with the relatively narrow width of the photoelectron spectral feature A. Similar to feature X, the fine structures in feature A also cannot be attributed to a single vibrational progression. It is also possible that there is more than one mode active during the detachment transition. The tentatively identified vibrational feature (~ 7100 cm^{-1}) is in reasonable accord with our calculated 806 cm^{-1} mode (see Table 1).

Table 2
Symmetry and eigenvalues of the top five occupied orbitals for the ground state MnO_4^- (T_d, $^1A_1$)

Orbital	− Eigenvalues (eV)	ΔE (eV)
$1t_1^6$	1.78	0.0
$6t_2^6$	3.14	1.36
$6a_1^2$	3.84	2.06
$1e^4$	5.34	3.56
$5t_2^6$	5.53	3.75

Table 3
Observed and theoretical adiabatic electron binding energies and spectroscopic constants for MnO_4. Binding energies (BE) and term values (T_0) are in eV, and vibrational frequencies are in cm^{-1}

State	BE		T_0		Frequency	
	Expt.	Theory	Expt.	Theory	Expt.	Theory
X	4.80 ± 0.10[a]	4.96	0.0	0.0	800 ± 80	829
A	6.05 ± 0.06[b]	6.29	1.25	1.33	700 ± 80	806

[a] Vertical binding energy: 4.91 ± 0.03 eV.
[b] Vertical binding energy: 6.11 ± 0.03 eV.

Further insight can be obtained about the photoelectron spectrum of MnO_4^- on the basis of its occupied molecular orbitals and the single-particle photodetachment picture. Table 2 shows the top few molecular orbitals of the MnO_4^- ground state. The X feature in the photoelectron spectrum can be viewed as removal of an electron from the $1t_1$ HOMO of MnO_4^-. This would produce a degenerate electronic state ($^2T_1$), which is expected to undergo Jahn–Teller distortions to the C_{2v} MnO_4. The degenerate $^2B_1$ and $^2B_2$ states of the ground-state MnO_4 (Fig. 1a) should correspond to the components of the $^2T_1$ state. The Jahn–Teller effects may also contribute to the complication of the X feature. Table 3 suggests that the feature A should be derived from removal of an electron from the $6t_2$ (HOMO-1) orbital of MnO_4^-. It is interesting that even the relative energy of the $6t_2$ orbital (1.36 eV) is in excellent agreement with the observed A–X separation (1.25 eV). The removal of a $6t_2$ electron would also result in a degenerate electronic state ($^2T_2$), which should also undergo Jahn–Teller distortions. The D_{2d} $^2A_1$ state may be considered a component of the $^2T_2$ state and the Jahn–Teller effects should also contribute to the complexity of the observed A feature (Fig. 4). The relatively small geometrical changes upon removing either a HOMO or HOMO-1 electron are not surpris-

ing because both the $1t_1$ and $6t_2$ orbitals are localized on the O atoms and are nonbonding orbitals. The latter is mainly responsible for the relatively narrow photoelectron spectral features (Fig. 4) observed despite the anticipated Jahn–Teller effects, which usually would result in much broader and more complicated spectral features. The relatively small geometrical changes upon photodetachment of MnO_4^- are also a manifestation of the strong Mn–O chemical bonding.

Table 3 summarizes the experimental spectroscopic values compared to those from the theoretical calculations. The excellent agreement between the predicted values and experimental measurements is indeed gratifying. This level of agreement clearly demonstrates the power of the present theory, which cannot only explain experimental observations, but also be predictive in nature. Our prediction of the existence of a peroxide isomer of MnO_4^- as well as the quenching of the magnetic moment with successive addition of oxygen can be verified in low-temperature matrix isolation experiments involving infrared spectroscopy and electron spin resonance. We hope this work will stimulate such investigations.

This work was supported in part (P.J. and B.K.R.) by a grant from the Department of Energy (Grant No. DE-FG02-96ER45579). The experimental work (L.S.W.) was supported by NSF (CHE-9817811). The experiment was performed at the W.R. Wiley Environmental Molecular Sciences Laboratory, a national scientific user facility sponsored by DOE's Office of Biological and Environmental Research and located at Pacific Northwest National Laboratory, which is operated for DOE by Battelle under Contract DE-AC06-76RLO 1830. L.S.W. is an Alfred P. Sloan Foundation Research Fellow.

References

[1] G.L. Gutsev, A.I. Boldyrev, Adv. Chem. Phys. 61 (1985) 169.
[2] F.A. Cotton, G. Wilkinson, Advanced Inorganic Chemistry, Wiley–Interscience, New York, 1988.
[3] R.R. Squires, Chem. Rev. 87 (1987) 623.
[4] R.H. Fokkens, I.K. Gregor, N.M.M. Nibbering, Rapid Commun. Mass Spectrom. 5 (1991) 368.
[5] E.B. Rudnyi, E.A. Kaibicheva, L.N. Sidorov, Rapid Commun. Mass Spectrom. 7 (1993) 800.
[6] G.L. Gutsev, A.A. Levin, J. Struct. Chem. (Russian translation) 20 (1979) 663.
[7] R.M. Dickson, T. Ziegler, Int. J. Quantum Chem. 58 (1996) 681.
[8] H. Nakai, Y. Ohmori, H. Nakatsuji, J. Phys. Chem. 99 (1995) 8550.
[9] G.L. Gutsev, A.I. Boldyrev, Chem. Phys. Lett. 108 (1984) 255.
[10] H. Johansen, Mol. Phys. 49 (1983) 1209.
[11] M.A. Buijse, E.J. Baerends, J. Chem. Phys. 93 (1990) 4129.
[12] G.L. Gutsev, A.I. Boldyrev, Chem. Phys. 56 (1981) 277.
[13] W. Kohn, L.J. Sham, Phys. Rev. 140 (1965) A1133.
[14] A.D. Becke, Phys. Rev. A 38 (1988) 3098.
[15] J.P. Perdew, Y. Wang, Phys. Rev. B 45 (1992) 13244.
[16] GAUSSIAN94, Revision B.1, M.J. Frisch, G.W. Trucks, H.B. Schlegel, P.M.W. Gill, B.G. Johnson, M.A. Robb, J.R. Cheeseman, T. Keith, G.A. Petersson, J.A. Montgomery, K. Raghavachari, M.A. Al-Laham, V.G. Zakrzewski, J.V. Ortiz, J.B. Foresman, J. Cioslowski, B.B. Stefanov, A. Nanayakkara, M. Challacombe, C.Y. Peng, P.Y. Ayala, W. Chen, M.W. Wong, J.L. Andres, E.S. Replogle, R. Gomperts, R.L. Martin, D.J. Fox, J.S. Binkley, D.J. Defrees, J. Baker, J.P. Stewart, M. Head-Gordon, C. Gonzalez, J.A. Pople, Gaussian, Pittsburgh, PA, 1995.
[17] M.J. Travers, D.C. Cowles, G.B. Ellison, Chem. Phys. Lett. 164 (1989) 449.
[18] L.S. Wang, C.F. Ding, X.B. Wang, S.E. Barlow, Rev. Sci. Instrum. 70 (1999) 1957.
[19] K.P. Huber, G. Herzberg, Constants of Diatomic Molecules, Van Nostrand–Reinhold, New York, 1979.
[20] G. Palenik, Inorg. Chem. 6 (1967) 503.
[21] H. Homborg, Z. Anorg. Allgem. Chem. 498 (1983) 25.
[22] G.L. Gutsev, S.N. Khanna, B.K. Rao, P. Jena, Phys. Rev. A 59 (1999) 3681.
[23] H. Wu, S.R. Desai, L.S. Wang, J. Am. Chem. Soc. 118 (1996) 5296.
[24] H. Wu, L.S. Wang, J. Chem. Phys. 108 (1998) 5310.
[25] G.L. Gutsev, R.J. Bartlett, A.I. Boldyrev, J. Simons, J. Chem. Phys. 108 (1997) 3867.
[26] G.L. Gutsev, P. Jena, R.J. Bartlett, Chem. Phys. Lett. 292 (1998) 289.
[27] X.B. Wang, C.F. Ding, L.S. Wang, A.I. Boldyrev, J. Simons, J. Chem. Phys. 110 (1999) 4763.
[28] S.K. Nayak, P. Jena, J. Am. Chem. Soc. 121 (1999) 644.